

Lecture 3

ENSO's irregularity and phase locking

Eli Tziperman

3.1 Is ENSO self-sustained? chaotic? damped and stochastically forced?

That El Niño is aperiodic is seen, for example, in a Niño-3.4 time series (Fig. 26). The ENSO delayed oscillator mechanism may result in either self-sustained oscillations, or in a steady state solution that has a damped oscillatory mode. In the latter case, oscillations may be excited by external stochastic (weather) noise. In the scenario in which ENSO is self-sustained, it may be irregular due to low-order chaos. In the stochastically driven scenario, ENSO's irregularity is simply an outcome of the stochastic forcing. Whether ENSO is damped or self-sustained depends on the ocean-atmosphere coupled instability, also referred to as the coupling strength. For this purpose, the coupling strength may be defined for example as the response of the atmospheric wind stress per unit change in the thermocline depth. Note that this coupling is the product of (at least) three different coupling coefficients: the response of SST to thermocline depth changes, the response of the atmospheric heating to SST changes, and the response of the wind stress to the atmospheric heating. A stronger coupling implies self-sustained possibly chaotic oscillation, while a weak coupling implies damped oscillations.

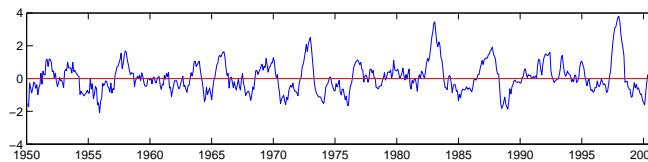


Figure 26: The observed irregular El Niño events (Niño-3.4 index of averaged east equatorial SST).

3.1.1 Strength and seasonality of ocean-atmosphere coupling

Some of the physical processes affecting the coupling strength are the mean (i.e. monthly climatological) upwelling strength, mean SST; ITCZ motion and its effect on the atmospheric heating parameterization, mean thermocline depth, thermocline outcropping, etc [23, 46, 62]. All of these fields vary seasonally (Fig. 27), and therefore so does the coupling coefficient.

To summarize only a few of the seasonal coupling factors:

1. Seasonal motion of ITCZ and its effect on atmospheric heating (via mean atmospheric convergence): results in stronger coupling when the ITCZ is near the equator.
2. Seasonal variations in upwelling amplitude: affects the efficiency of transfer of thermocline signal to surface.
3. Seasonal variations in the mean SST, and its effect on atmospheric heating: warmer mean SST makes a given SST perturbation more effective in inducing atmospheric heating.
4. Seasonal motion of thermocline in the East Pacific: when the thermocline outcrops, Kelvin Waves manage to transfer the sub-surface temperature signal to the surface and affect the SST more efficiently.

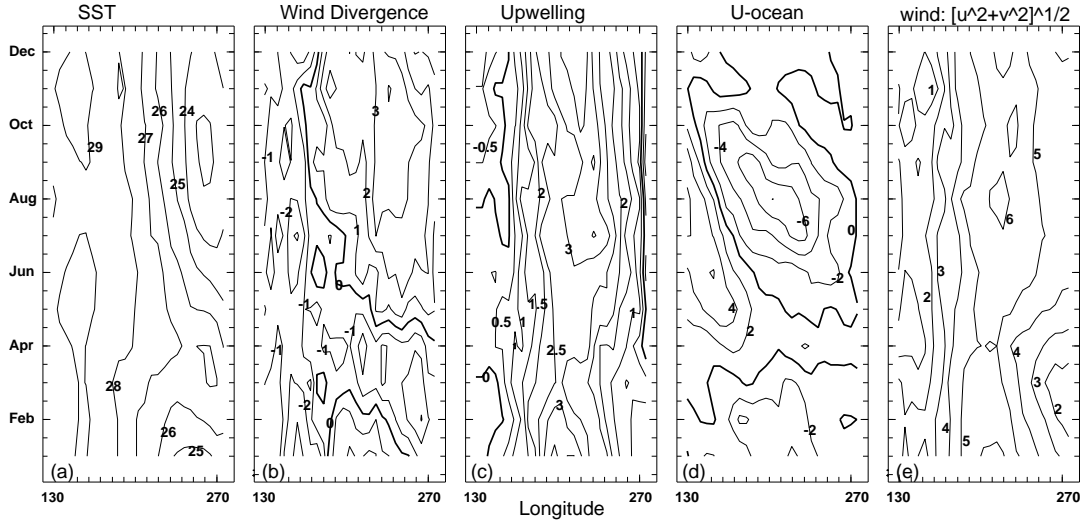


Figure 27: Monthly climatology of SST, wind divergence, upwelling, zonal ocean currents, and wind speed, at the equator, taken from the background fields in the CZ model.

Each of these factors results in a somewhat different time of maximal coupling. The combined effect is a seasonal coupling strength that is maximal during spring and early summer and minimal at the end of the calendar year.

Consider next the two possible mechanisms leading to ENSO's irregularity and limited predictability.

3.1.2 ENSO's irregularity: low order chaos

Consider first a pendulum driven by periodic forcing and affected by friction. For small amplitude, one may linearize the equation of motion, and when the forcing frequency equals the natural frequency of the pendulum, a linear resonance occurs. For larger amplitude motion, the governing equation is nonlinear. Because of the nonlinearity, the period of the pendulum depends on its amplitude. In this case a "nonlinear resonance" may occur when the pendulum frequency ω is related to the forcing frequency ω_F as two integers: $\omega/\omega_F = n/m$ rather than only when the two frequencies are equal, as in the linear case. When the nonlinearity is sufficiently strong, the pendulum tends to change its amplitude a bit so that its frequency would also change, such that the frequency is related to that of the forcing as the ratio of two integers and a nonlinear resonance occurs. This is also called "mode locking" to the external forcing, and is the same phenomenon as of the "Huygens clocks" shown in Fig. 28. For larger yet nonlinearity, the governing equation of the pendulum has several different solutions that correspond to different nonlinear resonances, all for the same physical parameters (friction, gravity, length of pendulum, forcing amplitude, etc). Each of these possible nonlinear resonances is unstable, so that the pendulum does not remain near these solutions indefinitely, but oscillates near one of these frequencies for a while, but then escapes and jumps to another such nonlinear resonance with a different integer ratio with ω_F . The resulting motion is an irregular jumping between the different nonlinear resonances. This is the mechanism of chaos for the damped nonlinear pendulum forced by external periodic forcing [1]. Check the pendulum Java applets at <http://www.dartmouth.edu/~phys15/interact/pendulum.html> or <http://monet.physik.unibas.ch/~elmer/pendulum/spend.htm> for a nice demo.

The above dynamics may also be demonstrated using the simple circle map

$$\theta_{n+1} = \theta_n + \Omega + \frac{K}{2\pi} \sin(2\pi\theta_n)$$

which is an iterative map roughly representing a periodically forced pendulum [54]. Here θ_n is the angle of the pendulum at iteration n , Ω represents the periodic forcing, and the nonlinear term with amplitude $\frac{K}{2\pi}$ corresponds

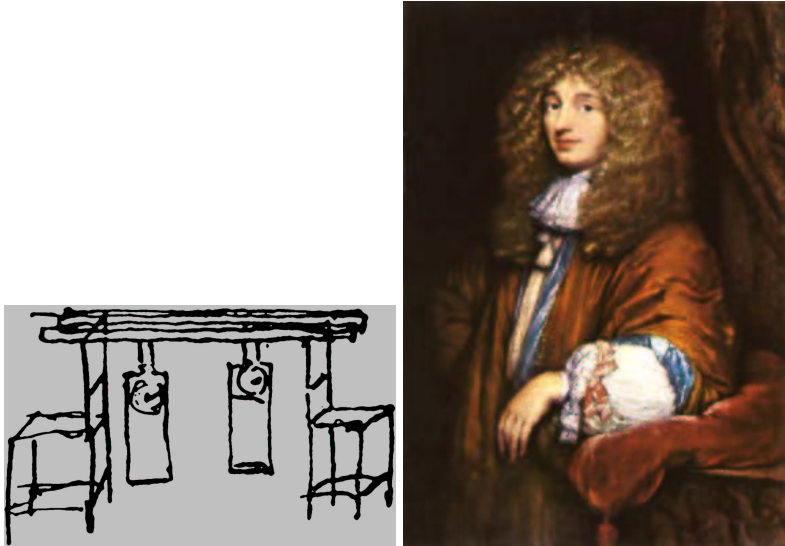


Figure 28: “While recovering from an illness in 1665, Dutch astronomer and physicist Christiaan Huygens noticed that two of the large pendulum clocks in his room (which he patented 8 years earlier) were beating in unison, and would return to this synchronized pattern regardless of how they were started, stopped or otherwise disturbed” (<http://www.agnld.uni-potsdam.de/~mros/synchro.html>).

to a similar term in the pendulum equation. As the nonlinearity in the map increases, the map displays a nonlinear resonance and then chaos for $K > 1$. The transition to chaos as the nonlinearity increases and as a function of Ω is called the quasi-periodicity route to chaos (Fig. 29); try playing with the following Matlab program to see the map behavior:

```
clear; clf; pi=atan(1.0)*4.0; omega=0.5; K=2.0; I=20000; theta(1:I)=1.0e-17;
for n=1:I
    theta(n+1)=mod(theta(n)+omega+(K/(2*pi))*sin(2*pi*theta(n)),1);
end
plot(theta,'r')
```

We finally proceed to the application of these ideas to ENSO’s dynamics. The idea is very simple [61, 58, 31]: the nonlinear pendulum in the above discussion corresponds to the delayed oscillator in a self-sustained parameter regime. The periodic forcing is the seasonal cycle and especially the seasonal variations of the coupling strength discussed above. This may be demonstrated by considering the transition to chaos in a simple delayed oscillator model [61] where the seasonal forcing is added as an additive forcing term,

$$\frac{dh(t)}{dt} = a\mathcal{A}[h(t - \frac{1}{2}\tau_K)] - b\mathcal{A}[h(t - \tau_K - \frac{1}{2}\tau_R)] + c \cos(\omega_a t) \quad (28)$$

and where $\mathcal{A}(h)$ is a nonlinear tanh-like function. This function has a slope of κ at the origin ($h = 0$) which serves as the coupling coefficient in the sense discussed above. As the coupling coefficient is increased, this model shows exactly the same quasi-periodicity route to chaos discussed above (Fig. 30). The same transition to chaos occurs if the seasonal forcing is added, more realistically, as seasonal variations in the coupling strength, rather than as an additive forcing term.

The mechanism of irregularity of El Nino according to this scenario is thus low order chaos driven by the seasonal cycle in the Equatorial Pacific. The nonlinear delayed oscillator goes into a nonlinear resonance with the seasonal cycle forcing. For sufficiently strong nonlinearity and/ or seasonal forcing amplitude, several such resonances coexist and are destabilized. Such a nonlinear resonance corresponds to an ENSO cycle of a period T_{ENSO} that is related to the annual period as the ratio of two integers. T_{ENSO} could be for example 2, 3 or 4 years,

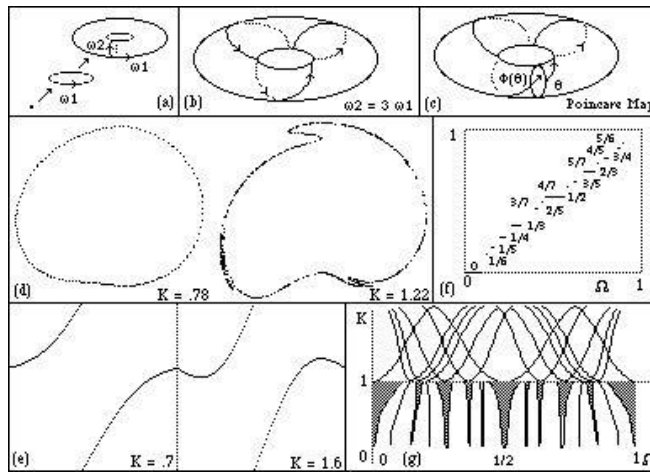


Figure 29: <http://www.dhushara.com/book/paps/chaos/bchaos1.htm>: “The quasi-periodicity route to chaos: (a) Repeated Hopf bifurcations result in tori. Creation of two oscillations results in a flow on the 2-torus. (b) Periodic flow on 2-torus results in closed orbits which meet themselves exactly. (c) Poincaré map of a cross section maps each point in a cross section C to the corresponding point one cycle on along the flow. The flow illustrated is irrational and hence has orbits consisting of lines which do not meet themselves, but cover the torus ergodically passing arbitrarily close as time increases. (d) Breakup of the torus under the circle map as K crosses 1. The increasing energy thus disrupts the periodic relationships as chaos sets in. (e) $f(q)$ versus q for the circle map. At $K = .7$ the function is $1 - 1$ and hence invertible, but for $K = 1.6$ it is not. (f) The devil's staircase of mode-locked states. These order the possible rationals assigning to each the interval of values for which such mode-locking occurs for $K = 1$. At this value the mode-locked states fill the interval, leaving only a Cantor set of irrational flows. (g) K - diagram of the circle map showing mode-locked tongues ($K < 1$) and chaos densely interwoven with periodicity ($K > 1$). The rational mode-locking exist only on the curves for $K > 1$.”

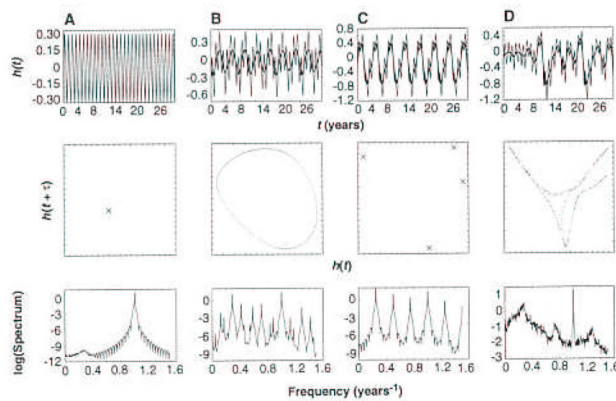


Figure 30: Transition to chaos in a simple delayed oscillator El Niño model [61].

or other period for which $T_{ENSO}/1yr = n/m$. The equatorial Pacific delayed oscillator therefore jumps irregularly between these nonlinear resonances, resulting in the observed irregularity. This scenario which was originally investigated using highly simplified toy models such as (28), was also found [58] to be the mechanism of chaos in the widely used El Nino prediction intermediate coupled model of Zebiak and Cane [66].

3.1.3 ENSO's irregularity: stochastically forced non-normal optimal modes

An alternative explanation to ENSO's irregularity is based on the idea of non normal transient growth [11, 10] and was examined in the context of ENSO for example by [45] and [32]. Consider first the simple linear system of two equations (thanks to Eyal Heifetz for his help with this example)

$$d\vec{\Psi}/dt = A\vec{\Psi}$$

where

$$A = \begin{pmatrix} -0.1 & -0.9 \cot \theta \\ 0 & -1 \end{pmatrix}$$

so that its eigenvectors/ values are

$$\begin{aligned} \vec{P}_1 &= \begin{pmatrix} 1 \\ 0 \end{pmatrix} \\ \vec{P}_2 &= \begin{pmatrix} \cos \theta \\ \sin \theta \end{pmatrix} \\ \begin{pmatrix} \lambda_1 \\ \lambda_2 \end{pmatrix} &= \begin{pmatrix} -0.1 \\ -1 \end{pmatrix}. \end{aligned}$$

Note that both eigenvalues are negative, so that the solution to any initial conditions eventually decays to zero. The solution may be written as

$$\vec{\Psi} = a_1 \vec{P}_1 e^{-0.1t} + a_2 \vec{P}_2 e^{-t},$$

where the initial conditions are

$$\vec{\Psi}(t=0) = a_1 \vec{P}_1 + a_2 \vec{P}_2.$$

At a later time $t = 1$, the solution is therefore

$$\vec{\Psi}(t=1) = a_1 \vec{P}_1 e^{-0.1} + a_2 \vec{P}_2 e^{-1}.$$

Now, note that the two eigenvectors are not necessarily perpendicular, depending on the value of θ :

$$\begin{aligned} \theta &= 0 \Rightarrow \vec{P}_1 \parallel \vec{P}_2; \\ \theta &= \pi/2 \Rightarrow \vec{P}_1 \perp \vec{P}_2 \end{aligned}$$

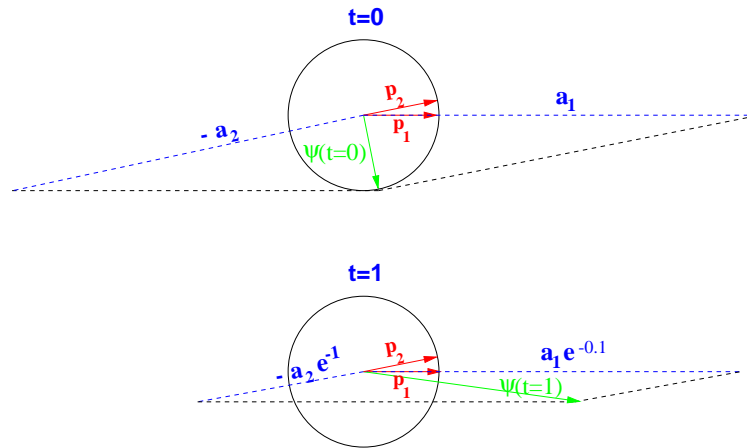
choosing initial conditions such that

$$\vec{\Psi}(t=0) = (\sin \theta, -\cos \theta)^\dagger \perp \vec{P}_2 \Rightarrow (a_1, a_2) = (\csc \theta, -\cot \theta)$$

we find that at a later time the norm of the solution actually increased rather than decay

$$\theta = \pi/18_{rad} = 10^\circ \Rightarrow |\vec{\Psi}(t=1)|/|\vec{\Psi}(t=0)| \approx 3.2$$

This somewhat surprising result may be explained with the help of Fig. 31. Note that the initial conditions are a super position of the two eigenvectors in such a way that the two components proportional to the eigen vectors



Non-modal transient growth: change in both amplitude and structure

Figure 31: non-normal system at i.c and at a later time

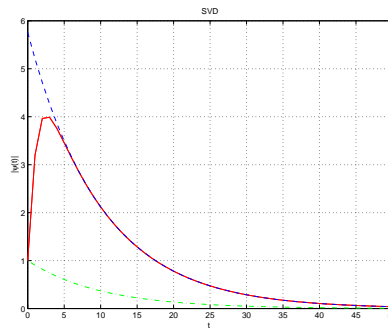


Figure 32: amplitudes as function of time for the projections on the eigenvectors (dash and dotted lines) and for the norm of the total solution (solid line).

are large-amplitude but cancel each other at $t = 0$. At a later time $t = 1$ one of the eigenvectors decays much faster than the other, so that the solution at that time remains basically equal to the large initial value of the remaining eigenvector, hence the initial amplification. This amplification is transient because at later times both eigenvectors must decay (Fig. 32).

Given a dynamical system as above, we could search for the initial conditions that maximize growth at some time $t = T_{opt}$, by solving the problem

$$\text{find } \Psi(t = 0) \text{ that results in } \max |\Psi(t = T_{opt})| \quad \text{subject to } |\Psi(t = 0)| = 1.$$

The usual normal modes stability analysis is equivalent to taking $T_{opt} \rightarrow \infty$. Alternatively, we could ask what are the initial conditions that lead to a maximum initial growth trend at $t = 0$

$$\text{find } \Psi(t = 0) \text{ that results in } \max \left| \frac{d\Psi}{dt} \Big|_{t=0} \right| \quad \text{subject to } |\Psi(t = 0)| = 1.$$

In this last case, we search for the maximum of the norm of $(d\Psi/dt)|_{t=0} = A\Psi(t = 0) = A\Psi_0$ subject to $|\Psi_0| = 1$. Writing this maximization problem using a Lagrange multiplier λ as

$$\begin{aligned} & \max ((A\Psi)^T (A\Psi) + \lambda(\Psi^T \Psi - 1)) \\ & = \max (\Psi^T (A^T A) \Psi + \lambda(\Psi^T \Psi - 1)). \end{aligned}$$

and equating the derivative of the quantity to be maximized and to zero, we have

$$\begin{aligned} 0 & = \frac{d}{d\Psi_0} (\Psi_0^T (A^T A) \Psi_0 + \lambda(\Psi_0^T \Psi_0 - 1)) \\ & = (A^T A) \Psi_0 + \lambda \Psi_0. \end{aligned}$$

This implies that the optimal initial conditions Ψ_0 that maximize the growth rate at $t = 0$ are the eigenvector of the matrix $A^T A$. In more general cases the answer is derived by solving different and somewhat more complex eigen problems, typically using an adjoint model of the model whose optimal initial conditions are searched.

As a final comment before returning to ENSO, note that if the optimal transient growth exceeds the non-linearity threshold within the time scale of interest, then the linear stability nature of the system is irrelevant. Very often the growth rate due to non-normal effects is much larger than that of the normal modes even for a system that is unstable in the usual normal modes sense. What's considered "optimal" is subjective.

In the case of ENSO, it has been suggested that the optimal initial conditions (e.g. for the wind) which result in the fastest growth of El Nino conditions (happen to?) have the same structure as of westerly wind bursts occurring in the West Pacific warm pool area (these wind bursts may be related to the Madden-Julian 30-40 day oscillations in the tropical atmosphere). This implies that El Nino may be triggered by external factors rather than being a self-sustained oscillation that is at most randomized by external noise. Predictability may still be possible if the system needs to be preconditioned before the westerly wind bursts can excite an event. In any case, the structure of the optimals for El Nino seems very model dependent at the moment, and the issue is still being investigated.

There are clearly many possible mechanisms for ENSO's irregularity, according to which it might be: self-sustained and chaotic, self-sustained and randomly forced; damped and stochastically forced efficiently due to the non-normal structure of its linearized dynamics, etc. At the moment, it seems that the issue of whether ENSO is self-sustained and possibly chaotic or damped and stochastically forced (or one of the other alternatives) is still unresolved.

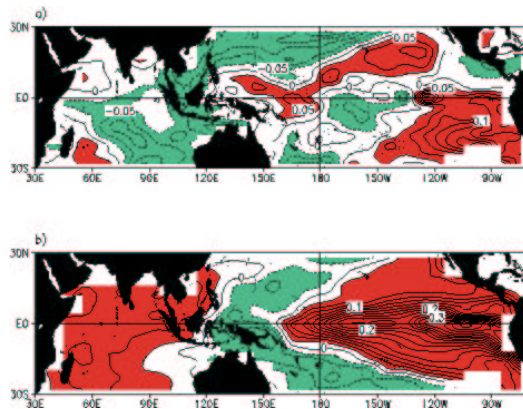


Figure 33: (a) The optimal initial structure for sea surface temperature anomaly growth. The pattern is normalized to unity. The contour interval is 0.025, and negative values are indicated by dashed contours. (b) The linear inverse model's 7-month prediction when (a) is used as the initial condition. Contour interval and shading are as in (a). (<http://www.cdc.noaa.gov/review97/overview/chpt2/fig.2.1.html>)

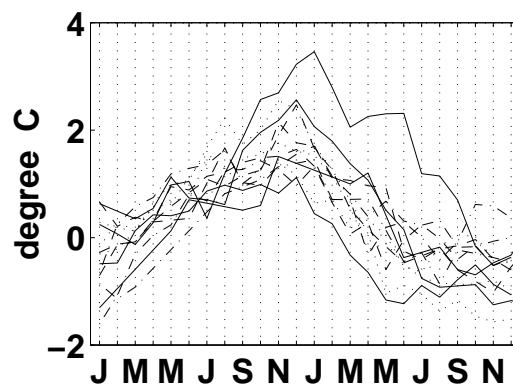


Figure 34: Super imposed nino3 time series from many observed events, showing the tendency of the events to reach a maximum toward the end of the year and therefore be phased locked to the seasonal cycle.

3.2 ENSO's phase locking to the seasonal cycle

El Nino events tend to reach their maximum toward the end of the year (Fig. 34). Given the importance of seasonal forcing via the seasonal ocean-atmosphere coupling strength to El Nino's dynamics it is not surprising that such phase locking occurs, but the mechanism of this phase locking still requires an explanation.

Some Previous explanations suggested that (1) Spring time is the most unstable time of year in the Equatorial Pacific, so that ENSO events start then & peak a few months later... (Philander [46], Hirst [23]). However, this explanation is clearly still a bit vague, summer is also unstable, and the delayed oscillator mechanism is not incorporated into the proposed mechanism. (2) End of year is most stable time of year, so that dissipation will overcome instability then, and events will peak and start decaying (Zebiak and Cane, [66]). However, this again does not use the equatorial waves and delayed oscillator ideas. (3) If El Nino's irregularity is due to seasonal forcing, one might expect nonlinear phase locking to the seasonal forcing. However, this is clearly not a sufficiently specific physical mechanism, and the locking actually seems to occur in linear models as well.

A linear mechanism based on equatorial wave dynamics for El Nino's phase locking has been proposed by [59, 12]. The mechanism may be demonstrated using a simple delayed oscillator equation

$$\begin{aligned}
 dh(t)/dt &= bF[K(t - \tau_1)h(t - \tau_1)] && \text{Warm Kelvin wave} \\
 &- cF[K(t - \tau_2)h(t - \tau_2)] && \text{Cold Rossby Waves} \\
 &- dh(t) && \text{Dissipation}
 \end{aligned} \tag{29}$$

where $h(t)$ = East Pacific thermocline depth, $K(t)$ = seasonal strength of ocean-atmosphere instability, $(\tau_1, \tau_2) = (1, 6)$ months, are the (Kelvin, Rossby+Kelvin) wave travel times, $F[K(t)h(t)]$ is a nonlinear function representing the thermocline \rightarrow SST \rightarrow wind connection, monotonously increasing with $K(t)h(t)$ and roughly shaped like a hyperbolic tangent function.

This model displays events that are aperiodic, but peak time of $h(t)$ (same as nino3), is always at the end of the year (Fig. 35).

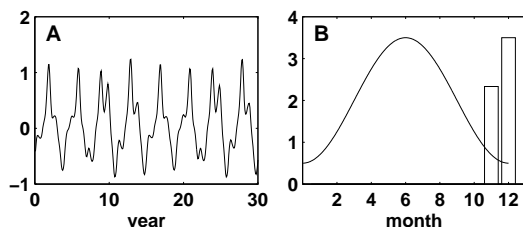


Figure 35: Results of the toy model described in the text for El Nino's phase locking. left: typical time series of model solution for $h(t)$; right: the seasonal coupling strength (line) and histogram of timing of peaks of the model time series showing that these peaks occur during November and December.

The end of year is also the time when the coupled ocean atmosphere instability strength (coupling strength) $K(t)$ is smallest in reality as well as in this toy model (solid line on right panel of Fig. 35). Given the simplicity of this model, we can try to use it to explain why the peak time is also time of minimum coupling. Note that at the peak time: $dh(t)/dt = 0$ so that warming due to the Kelvin wave term balances the cooling due to the Rossby and dissipation terms:

$$bF[K(t - \tau_1)h(t - \tau_1)] = cF[K(t - \tau_2)h(t - \tau_2)] + dh(t) \tag{30}$$

Next, we note that in the delayed oscillator picture, the ENSO cycle is viewed as a continuous succession of Kelvin and Rossby waves excited in the central Pacific. Also, the wave's initial amplitudes are related to that of the ENSO event at the time when the waves are excited. Finally, the waves are also amplified (during their excitation time) by the strength of the ocean-atmosphere instability at the season of their excitation.

Let us show now that the event peak cannot occur at a time of maximum ocean-atmosphere instability strength $K(t)$ (which is also summer time), using the schematic Fig. 36. If the peak time is indeed during summer, then warm Kelvin waves arriving during the peak time to the East Pacific are excited $\tau_1 = 1$ month before ENSO's peak-time with a large amplitude (because they are forced by a strong wind anomaly existing just prior to the peak time. These waves are also strongly amplified when they are excited by the strong coupling that exists during the summer. These strong waves cannot be balanced by the small-amplitude cold Rossby waves created $\tau_2 = 6$ months before the peak time, during the winter time, when the event was still weak, having also been only weakly amplified during winter by the weak coupled instability then. In other words, in equation (30), $K(t - \tau_1)$ and $h(t - \tau_1)$ are large, while $K(t - \tau_2)$ and $h(t - \tau_2)$ are small, so that the balance in that equation cannot be obtained, and therefore peak time cannot occur at the time of maximum coupling $K(t)$.

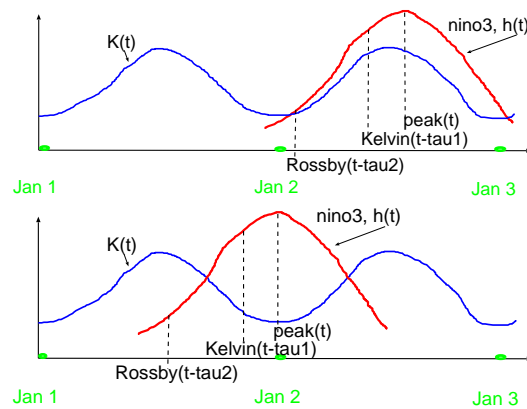


Figure 36: upper: can El Nino peak during summer time? lower: can El Nino peak during winter time? In both cases: the blue curve shows the seasonal coupling strength, and red curve the East Pacific SST.

Next, let us show that the peak can occur at a time of minimum ocean-atmosphere instability strength $K(t)$ (Fig. 36). In this case, the warm Kelvin waves arriving to the East Pacific at the peak time are Large amplitude because they were excited by the strong wind anomalies near the peak-time. But these waves were only weakly amplified during winter when they were excited. These waves may therefore be balanced by the cold Rossby waves excited with a small-amplitude when the event was still weak, but strongly amplified by the strong winter time coupled instability strength. In other words, in equation (30) we now have $K(t - \tau_1) = small$; $h(t - \tau_1) = large$, $K(t - \tau_2) = large$; $h(t - \tau_2) = small$, so that the balance in that equation may be obtained and peak time can occur at the time of minimum coupling $K(t)$. (Extension to mixed mode and other ENSO regimes were discussed by Galanti and Tziperman [12]).

The common bibliography for Eli Tziperman's lectures is at the end of Lecture 9, on page 131.